SIMULATION OF PREMATURE VENTRICULAR CONTRACTIONS IN PATIENT SPECIFIC BIDOMAIN VENTRICULAR MODEL

Elena Cocherová[1,2], Lukáš Zelieska[1,2], Milan Tyšler[1]

[1]Institute of Measurement Science, SAS, Bratislava, Slovakia

[2]Faculty of Electrical Engineering and Information Technology, STU, Bratislava, Slovakia

Abstract

The goal of the study was to simulate electrical activation of the heart ventricles and corresponding body surface potentials (BSPs) during premature ventricular contractions (PVC) using the patient specific realistic homogeneous model of cardiac ventricles and the torso. Real position of the initial ectopic activation during PVC was determined by intracardial measurement in the upper part of the right ventricle near the His bundle and confirmed by successful catheter ablation of the PVC origin. Simulated electrical activation in the ventricular model was started at the position of the initial ectopic activation as well as at several other sites at various distances from this position. The propagation of electrical activation in the ventricular model was modeled using bidomain reaction-diffusion (RD) equations with the ionic transmembrane current density defined by the modified FitzHugh-Nagumo (FHN) equations. The torso was modeled as a homogeneous passive volume conductor. The RD equations were numerically solved in the Comsol Multiphysics environment. Simulated ECG signals and BSPs were compared with those measured during PVC in a real patient. The polarity and shape of simulated and measured ECG leads as well as the BSP distribution during the PVC were in best agreement when the stimulated region was less than 10 mm from the position of the initial ectopic activation.

Keywords

bidomain reaction-diffusion model, realistic ventricles and torso model, premature ventricular contraction, ECG, body surface potentials

Introduction

Electrical activation of the heart ventricles is manifested on the torso in body surface potentials (BSPs). Their changes in time are represented in measured electrocardiographic (ECG) signals as the QRS complex.

In healthy heart, the electrical activation of the ventricles takes about 80 to 120 ms. It starts from the atrioventricular node and propagates through the conduction system to the working ventricular myocardium [1–2]. Since the velocity of activation propagation in the conduction system is about three times higher than that in the working ventricular myocardium, normal activation arrives rapidly during the first about 20 milliseconds at several endocardial regions of the healthy ventricular myocardium and spreads along the endocardium and toward the epicardium. During the first about 40 milliseconds about half of the ventricles is depolarized and ECG signals reach their maximal deflections.

In the pathologically changed heart, extraordinary ectopic electrical activation can start in the ventricles outside the conduction system and spread mainly through the working myocardium, resulting in a premature ventricular contraction (PVC)—extra-systole. The ectopic activation is reflected in changed BSP dynamics and the time needed to activate both ventricles represented by the QRS complex of the ECG signals is prolonged significantly over 120 ms. Patients with life-threatening frequent ventricular arrhythmias that do not respond to pharmacological treatment are indicated for catheter ablation of the arrhythmogenic tissue causing PVC. Several invasive and noninvasive methods can be used to obtain information about the PVC origin prior to the ablation procedure [3–5].

The goal of this study was to simulate electrical activation of the ventricles during ectopic stimulation and to obtain simulated ECG signals and BSP distribution as close as possible to the measured ones. If such stimulation position is identical or close to the real PVC origin, the model can help us to estimate the PVC origin noninvasively.

Lekar a technika – Clinician and Technology 2023, vol. 53(2), pp. 46–51, DOI: 10.14311/CTJ.2023.2.03
ISSN 0301-5491 (Print), ISSN 2336-5552 (Online)

Methods

In this study, we simulated the ectopic ventricular activation and corresponding ECG signals and BSP distribution during the PVC and compared them to data measured in a real patient. The model of ventricular activation was based on bidomain reaction-diffusion (RD) equations. BSPs were computed in a patient-specific homogeneous model of the torso and heart ventricles. Several stimulation positions simulating the initial ectopic ventricular activation were tested to obtain simulated ECG signals and BSP distribution similar to the measured ones.

Measured data

The data were recorded from a 17-year-old sportsman, a patient (P001) with frequent PVCs. ECG signals from limb leads and BSP maps from 128 electrodes on the chest were recorded for about 2 minutes. The geometry of torso and heart ventricles as well as real positions of measuring ECG electrodes were obtained from a CT scan of the torso taken immediately after the BSP measurement with ECG electrodes attached. The measurements were approved by the Ethical Committee of the National Institute of Cardiovascular diseases in Bratislava. Before the procedures, written informed consent was obtained from the patient. The patient was indicated to radiofrequency ablation of the ectopic focus in the electrophysiological lab. The ectopic focus was invasively localized by an intracardial catheter in the upper part of the septum near the His bundle and was confirmed by consequent successful ablation.

Model of the torso and heart ventricles

The model of the patient torso and heart ventricles as well as the positions of ECG electrodes (Fig. 1, Fig. 2) were obtained from the patient CT scan using the software TomoCon WORKSTATION (TatraMed Software, s.r.o., Slovakia) and Comsol Multiphysics (COMSOL A.B., Sweden).

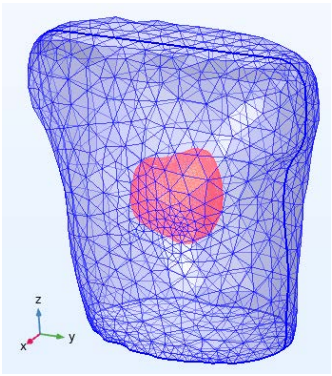

Fig. 1: The front view of the meshed model of the torso (blue) and the heart ventricles (red).

The size of the ventricular model was approximately 108 mm in base-to-apex direction (height), 115 mm in the left-to-right direction and 95 mm in the anterior-to-posterior direction. In the middle of the model height, the thickness of the wall was about 3–5 mm in the right ventricle, 9–11 mm in the left ventricle, and 9–11 mm in the septum.

The height of the torso was 380 mm, and cross-section dimensions at the level of the heart center were 303 mm and 216 mm. Torso was treated as a passive volume conductor with conductivity set to $\sigma = 0.02$ S/m.

The bidomain reaction-diffusion model

The propagation of electrical activation in the model of ventricles was simulated using bidomain RD equations with the ionic transmembrane current density defined by the modified FitzHugh-Nagumo (FHN) equations.

The bidomain RD model [6–8] is described by partial differential equations:

$$\frac{\partial V_e}{\partial t} - \frac{\partial V_i}{\partial t} + \nabla \cdot \left(- D_e \nabla V_e\right) = i_{ion} - i_s \,, \tag{1}$$

$$\frac{\partial V_i}{\partial t} - \frac{\partial V_e}{\partial t} + \nabla \cdot \left(- D_i \nabla V_i\right) = -i_{ion} + i_s \,, \tag{2}$$

where V_e is the extracellular potential, V_i is the intracellular potential, D_e and D_i are the extracellular and intracellular tissue diffusivity, i_{ion} is the normalized local ionic transmembrane current density, and i_s is the normalized stimulation current density. Current densities were normalized to the membrane capacitance.

The tissue diffusivity D (in this model $D = D_e = D_i$) is dependent on the tissue conductivity σ, on the membrane surface-to-volume ratio β, and on the membrane capacitance per unit area C_m:

$$D = \frac{\sigma}{\beta C_m} \,. \tag{3}$$

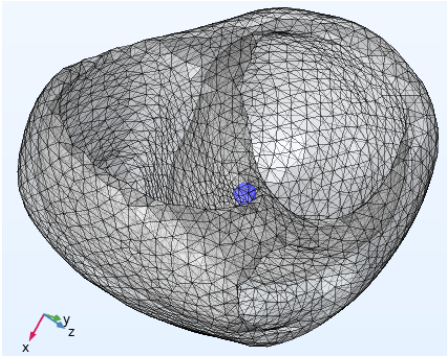

Fig. 2: The meshed model of the heart ventricles. The stimulated region (Pos45) in the upper part of the septum is highlighted in blue.

Lekar a technika – Clinician and Technology 2023, vol. 53(2), pp. 46–51, DOI: 10.14311/CTJ.2023.2.03
ISSN 0301-5491 (Print), ISSN 2336-5552 (Online)

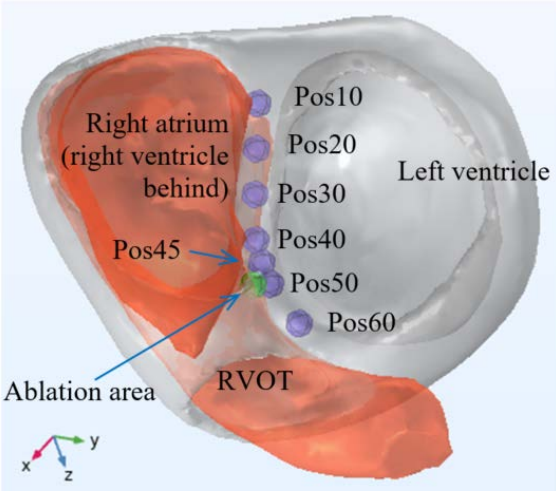

Fig. 3: Top view of the stimulated regions in the ventricular model (ablation area is highlighted in green, other positions in blue). For better spatial orientation, blood in the right atrium and right ventricular outflow tract (RVOT) (not included in the ventricular model) are figured as red.

The ionic transmembrane current density i_{ion} and the transmembrane potential ($V_m = V_i - V_e$) were modeled using the modified FHN equations [8, 9].

For homogeneous model of the ventricles, value of the tissue diffusivity in the myocardial tissue was set to $D = 0.0005$ m^2/s (corresponding to tissue conductivity $\sigma = 0.5$ S/m). Values of the modified FHN model parameters were the same as in [9]. For these parameters, the activation propagation velocity of a planar wave front was about 0.6 m/s. Initial value of the intracellular potential was set to –0.085 V and the other state variables were set to 0. Fluxes through all external boundaries of the torso were set to zero and the potential on the internal torso boundary with the ventricles was set to V_e.

The propagation of electrical activation in the ventricular model described by RD equations, and the BSPs in torso model were numerically solved in the Comsol Multiphysics environment.

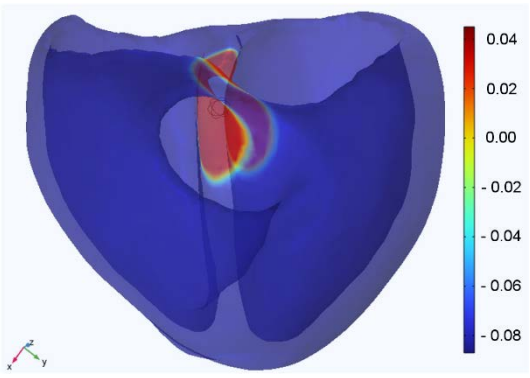

Fig. 4: The transmembrane potential V_m (V) in time t = 30 ms after the stimulation at position Pos45.

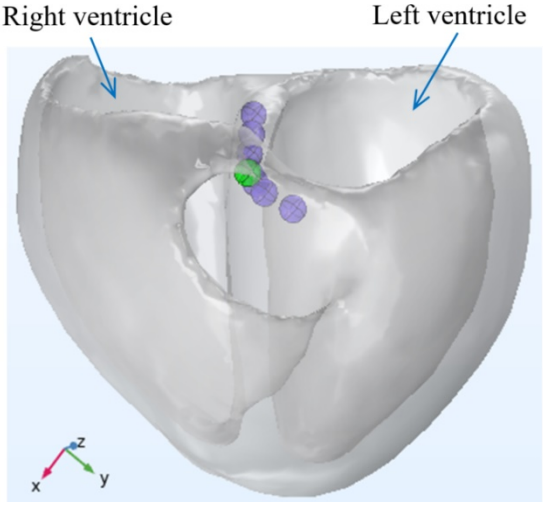

Fig. 5: Anterior view of the stimulated regions in the ventricular model (ablation area is highlighted in green, other positions are in blue).

Premature ventricular contraction modeling

The information about the PVC origin received from the measurements in electrophysiological lab was that the initial ectopic activation starts in the interventricular septum near the His bundle. The position of the catheter during successful ablation was in the right ventricular septum near the heart base.

For PVC modeling, several positions of the stimulated area in the upper part of the interventricular septum near the heart base were tested as possible PVC origin (Pos10 to Pos60, as shown in Fig. 3 and Fig. 4). Position Pos30 was selected approximately in the middle of the upper part of the septum. Positions Pos10 and Pos20 were 10 mm and 20 mm in posterior direction from the Pos30. Positions Pos40, Pos50 and Pos60 were 10 mm, 20 mm, and 30 mm in anterior direction from the Pos30. Position Pos45 was 15 mm in anterior direction from the position Pos30. We also used the position of the catheter during successful ablation (shown as green sphere in Fig. 3 and Fig. 4).

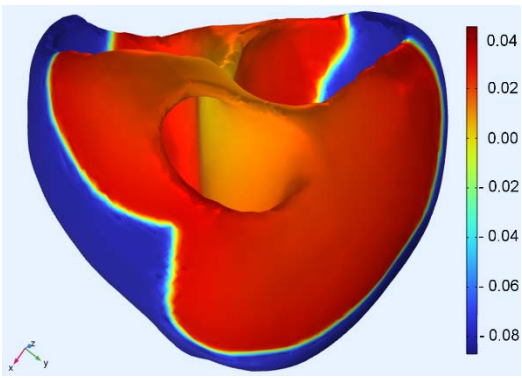

Fig. 6: The transmembrane potential V_m (V) in time t = 120 ms after the stimulation at position Pos45.

Lekar a technika – Clinician and Technology 2023, vol. 53(2), pp. 46–51, DOI: 10.14311/CTJ.2023.2.03
ISSN 0301-5491 (Print), ISSN 2336-5552 (Online)

Each tested site of supposed initial ectopic activation was modeled as a spherical region with a radius of 3 mm where the stimulation current was injected. If the site center was closer than 3 mm to the ventricular surface, the stimulation site was modeled as an intersection of the sphere with the ventricular tissue. The "smoothed rectangular" pulse with a duration of 10 ms and an amplitude of 40 A/F was used for stimulation.

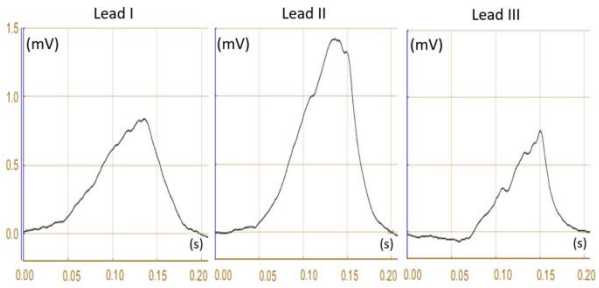

Fig. 7: The ECG potentials (mV) measured in limb leads I, II and III during QRS complex.

Results

The transmembrane potential V_m, ECG signals, and BSP distribution were numerically solved for the tested positions of the stimulated sites (shown in Fig. 3) as possible origins of ectopic activations. For example, spatial distribution of the simulated transmembrane potential V_m in selected time instants after the stimulation at position Pos45 is shown in Fig. 5 and Fig. 6.

The main criteria for comparison of the measured and simulated ECG signals were the polarities, relative amplitudes, and timing of the ECG signals in limb leads I, II and III.

During the QRS complex, polarity of all three measured ECG signals was positive, only very small negative polarity in limb lead III was observed during the first third of the QRS complex (Fig. 7). Amplitudes of measured limb leads I and III were slightly above 50% of the limb lead II amplitude.

The onset of the limb lead III was delayed after the onset of the limb leads I and II.

The simulated ECG signals corresponding to stimulation at positions Pos10, Pos20 and Pos30 did not satisfy the polarity criterion, as the polarity of limb lead III was negative during considerable part of the QRS complex (Fig. 8).

Simulated ECG signal corresponding to stimulation at position Pos60 did not satisfy the amplitude criterion, as the amplitude of limb lead III was nearly as high as that of limb lead II.

For simulated ECG signals corresponding to stimulation at the remaining tested positions Pos40, Pos45 and Pos50, the amplitude criterion was relatively well met for position Pos45, as the shapes of the ECG signals were most similar to the measured ones.

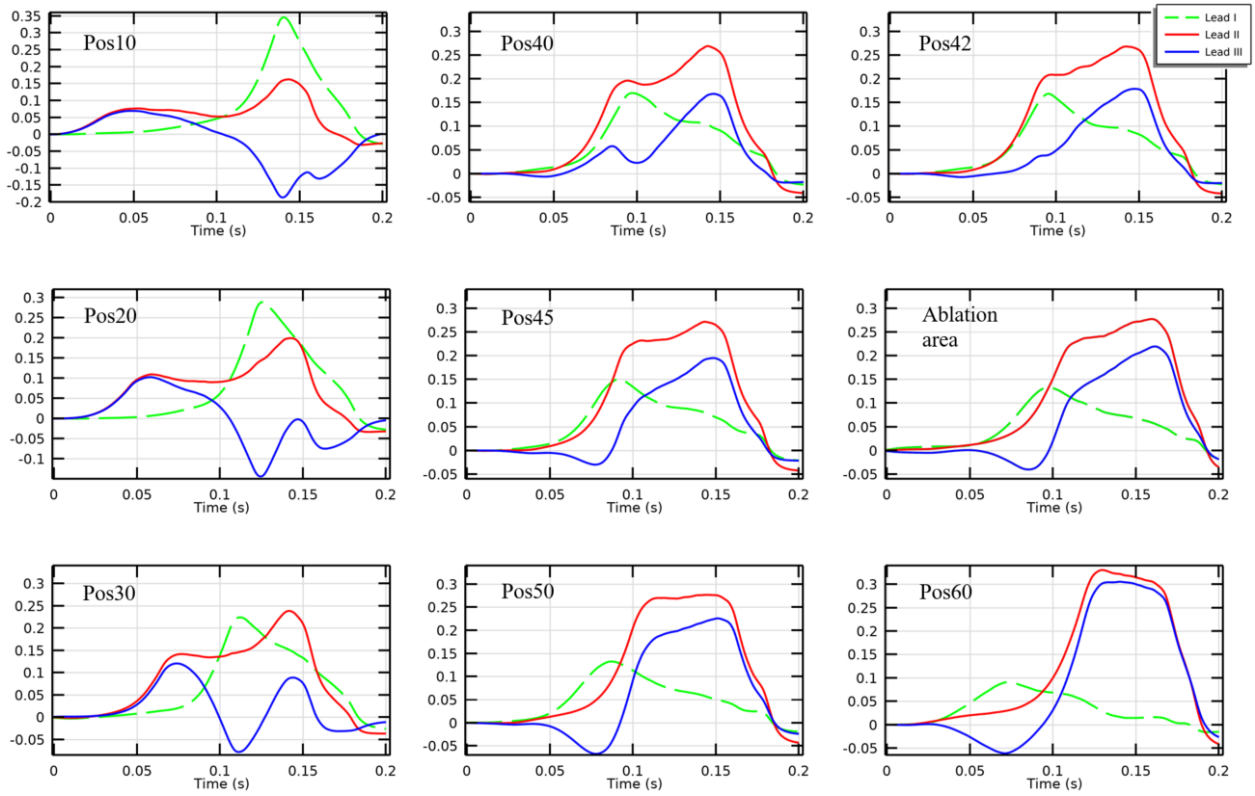

Fig. 8: The simulated potentials (mV) in limb leads I, II and III during QRS complex in ECG.

Lekar a technika – Clinician and Technology 2023, vol. 53(2), pp. 46–51, DOI: 10.14311/CTJ.2023.2.03
ISSN 0301-5491 (Print), ISSN 2336-5552 (Online)

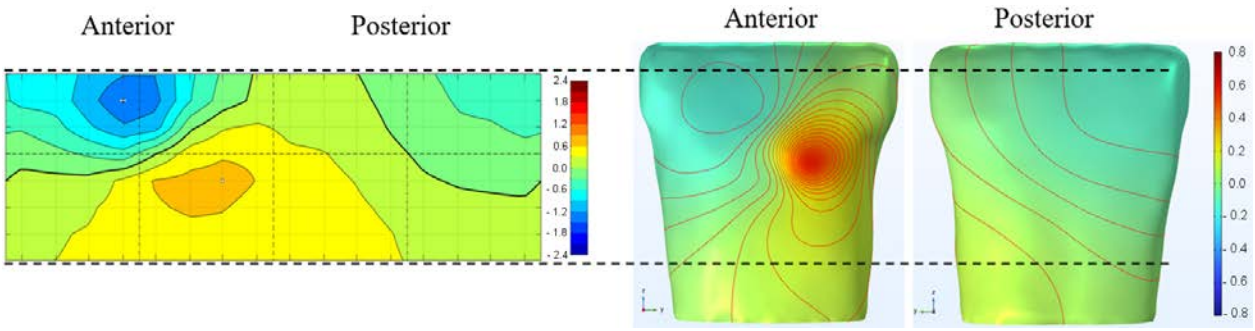

Fig. 9: Measured BSP map (mV) (left and the corresponding simulated BSP (mV) (right) in time t = 100 ms after the stimulation at position Pos45. Dashed lines show the range of the torso covered with ECG electrodes.

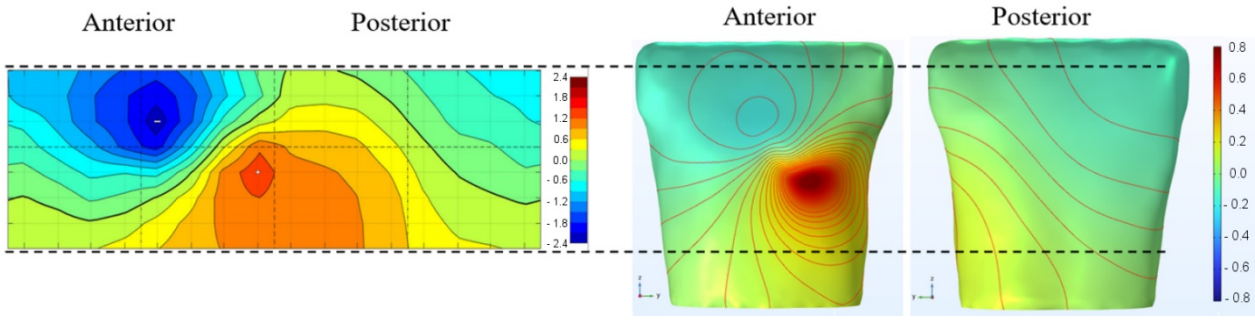

Fig. 10: Measured BSP map (mV) (left) and the corresponding simulated BSP (mV) (right) in time t = 135 ms after the stimulation at position Pos45. Dashed lines show the range of the torso covered with ECG electrodes.

From the tested stimulation positions shown in Fig. 3, the best agreement between measured and simulated ECG signals according to the predefined criteria was obtained for stimulation at position Pos45 and at the position of the ablation site.

In addition, other stimulation points in the vicinity (within 3 mm) of the best evaluated positions were also tested and, according to the mentioned criteria, a good agreement with the measured data was achieved. For example, simulated ECG for stimulation at position Pos42 (shifted 3 mm posteriorly from Pos45) is shown in Fig. 8. The distance between the center of ablation area and positions Pos45 and Pos42 was 7.3 mm and 9.6 mm, respectively.

The distribution of measured and simulated BSP in time instants 100 ms and 135 ms after stimulation at position Pos45 is shown in Fig. 9 and Fig. 10. The measured and corresponding simulated BSP maps have similar basic patterns and their dynamics: The minimum was situated in the upper anterior part of the torso, slightly to the right from the midsternal line and it increased and moved slightly to the left, while the maximum was in the lower anterior part of the torso and it increased without any significant change of position.

Discussion

ECG signals and BSP distributions obtained from simulated PVCs with stimulation at position Pos45 or at the position of the ablation site were most similar to the measured ones. When looking on the QRS complexes in simulated limb leads signals, the peaks of positive polarity were correctly occurring in all limb leads, with highest maximum in limb lead II and with delayed onset in limb lead III.

In both, simulated and measured data during PVC, ECG signals in all limb leads have initial flat part followed by less steep course when compared with the ECG during normal heartbeats. This can be explained by the position of the PVC origin (near heart base where there is no conduction system) and by the fact that during PVC the activation is spreading in the working myocardium, not in the conduction system.

Differences between the measured and simulated ECGs and BSPs, can be caused by not considering the torso inhomogeneities, myocardium anisotropy and by not taking into account the possible partial role of the fast conduction system. During the ectopic ventricular activation, it is difficult to predict whether the activation will spread only in the working myocardium, or if it will also enter the conduction system. In this patient, the role of the conduction system seems to be minor, at least during the initial part of the QRS complex.

Lekar a technika – Clinician and Technology 2023, vol. 53(2), pp. 46–51, DOI: 10.14311/CTJ.2023.2.03
ISSN 0301-5491 (Print), ISSN 2336-5552 (Online)

Conclusion

We can conclude that the simulation of the ectopic ventricular activation can produce ECG signals in limb leads I, II and III and BSP distribution close to the measured data. Best agreement between simulated BSP and BSP measured during PVC was obtained when the stimulation positions modeling the initial ectopic ventricular activation were up to about 10 mm from the real PVC origin determined by the intracardial mapping and successful ablation in the electro-physiological lab.

The results suggest that modeling can be quite successful in noninvasive estimation of PVC foci situated outside the ventricular conduction system based on BSP measured during the extrasystole and using realistic homogeneous model of the patient torso and ventricles.

Some differences between simulated and measured ECG signals may possibly be reduced by further model improvement by adding torso inhomogeneities, myocardium anisotropy and conduction system involvement.

Acknowledgement

The work was supported by research grant APVV-19-0531 from the Slovak Research and Development Agency and grant VEGA 2/0109/22 from the VEGA grant agency.

References

[1] Malmivuo J, Plonsey R. Bioelectromagnetism: Principles and Applications of Bioelectric and Biomagnetic Fields. New York: Oxford University Press; 1995. DOI: 10.1093/acprof:oso/9780195058239.001.0001

[2] Macfarlane PW, van Oosterom A, Pahlm O, Kligfield P, Janse M, Camm J. Comprehensive Electrocardiology. London: Springer Science & Business Media; 2010. 2291 p. DOI: 10.1007/978-1-84882-046-3

[3] van Dam PM, Tung R, Shivkumar K, Laks M. Quantitative localization of premature ventricular contractions using myocardial activation ECGI from the standard 12-lead electrocardiogram. Journal of Electrocardiology. 2013 Nov–Dec;46(6):574–9. DOI: 10.1016/j.jelectrocard.2013.08.005

[4] Tysler M, Svehlikova J, Deutsch E, Osmancik P, Hatala R. Noninvasive Imaging of the Origin of Premature Ventricular Activity. In: Lhotska L, Sukupova L, Lacković I, Ibbott GS, editors. IFMBE Proceedings. World Congress on Medical Physics and Biomedical Engineering 2018; 2018 Jun 3–8; Prague, Czech Republic. Singapore: Springer Singapore; 2019. p. 97–101. DOI: 10.1007/978-981-10-9035-6_18

[5] Bear LR, Dogrusoz YS, Good W, Svehlikova J, Coll-Font J, van Dam E, et al. The Impact of Torso Signal Processing on Noninvasive Electrocardiographic Imaging Reconstructions. IEEE Transactions on Biomedical Engineering. 2021 Feb; 68(2):436–47. DOI: 10.1109/TBME.2020.3003465

[6] Potse M, Dube B, Richer J, Vinet A, Gulrajani RM. A Comparison of Monodomain and Bidomain Reaction-Diffusion Models for Action Potential Propagation in the Human Heart. IEEE Transactions on Biomedical Engineering. 2006 Dec;53(12):2425–35. DOI: 10.1109/TBME.2006.880875

[7] Clayton RH, Bernus O, Cherry EM, Dierckx H, Fenton FH, Mirabella L, et al. Models of cardiac tissue electrophysiology: Progress, challenges and open questions. Progress in Biophysics and Molecular Biology. 2011 Jan;104(1–3):22–48. DOI: 10.1016/j.pbiomolbio.2010.05.008

[8] Sovilj S, Magjarevic R, Lovell NH, Dokos S. A Simplified 3D Model of Whole Heart Electrical Activity and 12-Lead ECG Generation. Computational and Mathematical Methods in Medicine. 2013 Apr 22;2013:134208. DOI: 10.1155/2013/134208

[9] Cocherová E. Analysis of the activation propagation velocity in the slab model of the cardiac tissue. In: Manka J, Tysler M, Witkovský V, Frollo I, editors. Measurement 2015. 10th International Conference on Measurement; 2015 May 25–28; Smolenice, Slovakia. Bratislava: Institute of Measurement Science, SAS; 2015. p. 105–8.

Ing. Elena Cocherová, Ph.D.
Department of Biomeasurements
Institute of Measurement Science
Slovak Academy of Sciences
Dúbravská cesta 9, 841 04 Bratislava

E-mail: elena.cocherova@savba.sk
Phone: +421 915 484 264

Lekar a technika – Clinician and Technology 2023, vol. 53(2), pp. 46–51, DOI: 10.14311/CTJ.2023.2.03
ISSN 0301-5491 (Print), ISSN 2336-5552 (Online)